# NUMERICAL SIMULATION OF THE MECHANICALLY COUPLED COOK-OFF EXPERIMENT

Jobie M. Gerken[1] (jgerken@lanl.gov)
Joel G. Bennett[2] (jbennett@lanl.gov)
Los Alamos National Laboratory
Engineering Sciences & Applications Division
Engineering Analysis Group
MS P946
Los Alamos, New Mexico 87545
PH: (505) 665-5758
FAX: (505) 665-2137

F. W. Smith[2], PE (fred@engr.colostate.edu)
Colorado State University
Department of Mechanical Engineering
Fort Collins, Colorado 80523
PH: (970) 491-6558
FAX: (970) 491-3827

[1] Associate Member, ASME
[2] Fellow, ASME

## Abstract

There has been a significant amount of recent interest concerning the behavior of High Explosives including work on an experiment known as the Mechanically Coupled Cook Off experiment in which a confined sample of polymer bonded explosive is heated and then ignited. This paper presents a finite element simulation of that experiment and provides comparisons with the experimental results. The numerical simulation includes elastic-plastic behavior of the confinement, thermal expansion effects, the mechanical and thermal response of the explosive, and a discrete crack propagation model. The results of the numerical simulation show that the general features of the experiment are reproduced.

## Introduction

High explosives (HE) are used in a variety of applications and unexpected explosions of HE could have significant consequences. Because of this, the response of HE to a variety of dynamic loading conditions which might be encountered in real-world situations is of significant interest and is being studied extensively [1 - 3]. Until recently, the response of these materials in specific practical engineering situations has been predicted based upon the results of extensive experimentation [4,5]. However, recent advances in numerical modeling techniques have shown promise for predicting the response of HE in such situations. The numerical models in use are in various stages of development thus making validation of such models very important. Numerical models

need to be robust and be able to reproduce experimental results, otherwise, there is no reasonable expectation that the models would provide accurate results when used to predict HE behavior in practical engineering situations.

The work presented in this report is an effort to validate some of the currently available finite element models. These models are being used to predict the response of HE by numerically predicting the results of one type of experiment which is performed on the energetic particulate HE material known as PBX 9501 [6]. The experiment, known as the Mechanically Coupled Cook Off (MCCO) experiment, is one in which the "cook-off" of PBX 9501 is reproduced by confining a small circular slab of the HE material in a circular metal ring and then subjecting the assembly to a uniform temperature increase. As the temperature increases, the HE undergoes a transition from a response that is primarily thermo-mechanical in nature to a response that is characterized by coupled mechanical, thermal and chemical reaction behaviors occurring under highly dynamic conditions. The early stages of this complex behavior are recorded using various techniques, the most informative of which is optical photography. The photographs that result from an experiment show that on the order of 3 to 5 distinct narrow zones of luminous activity propagate through the PBX 9501. These luminous zones have been postulated to be the ignition of newly exposed HE surface as discrete cracks propagate through the HE [6].

The numerical modeling of such an experiment is a difficult task. To predict the behavior observed in the experiments, many different phenomena must be incorporated into the numerical model. The finite element model developed to simulate these experiments incorporates many of the salient features. Thermal straining has been

incorporated into the model to reproduce the stress field and the deformation which occur due to the thermal expansion mismatch between the metal and the HE. The magnitude of the stress field in the metal confinement becomes large enough that it must be modeled as an elastic-plastic material. A new visco-elastic damage model, called ViscoSCRAM, has been developed to model the mechanical response of PBX 9501 [7]. A new method for modeling discrete cracking in a finite element mesh is used to model the macroscopic crack propagation in the HE [8]. These methods have all been incorporated into ABAQUS/Standard, an implicit dynamic finite element code, selected as appropriate for modeling the geometric, material and dynamic behaviors that must be included to capture the experimental features.

## The MCCO Experiment

The terminology “cook off” refers to an event involving HE, in which the temperature of the HE is increased due to fire or some other heating influence. The practical engineering concern in such events is that the HE may explode under these conditions at a critical temperature in the absence of any mechanical disturbance, or that an explosion may occur at a temperature below the critical level in the presence of a mechanical disturbance.

A schematic of the MCCO experiment is shown in Fig. 1. A small flat cylinder of PBX 9501 is confined in a metal ring of copper or mild steel of various thicknesses (6.35 mm, 3.175 mm, and 1.588 mm have been used). The HE and ring assembly is confined between a window at the top and a solid metal surface at the bottom. The HE specimen

has an outer diameter of 25 mm and an inner diameter of 3.175 mm. To simulate the cook-off event, the cylinder of HE is heated uniformly from both the top and bottom. In some cases, the sample is heated to auto-ignition. For the experiments simulated here, the sample is heated to a temperature below the auto-ignition temperature, at which point ignition is initiated at the inner surface of the cylinder by means of an electrically heated NiCr wire.

Experimental observations are made in several ways including the use of a camera that photographs the HE at intervals of 3 to 5 $\mu$sec through the top window. The sequence of photographs presented in Fig. 2 shows the behavior of HE in a MCCO experiment after the onset of the chemical reaction. The specimen was confined in a 3.175mm thick copper ring, heated to 190°C in about 1 hour, and ignited with a NiCr wire. The photographs show narrow regions of lumination propagating from the inner surface outward toward the confinement ring. This lumination is thought to be caused by the ignition of fresh HE surface behind discrete cracks as they propagate radially outward from the inner surface of the specimen [6]. The photographs show that early in the process, at about 0 to 5 $\mu$sec after the start of observation, there appear to be three narrow cracks starting to propagate outward. The largest of the three cracks then branches into two different cracks at about 10 $\mu$sec, still propagating in a somewhat radial direction. As time progresses, much of the HE has started to chemically react and the lumination overwhelms the details of discrete cracks and branching phenomena observed earlier. In this experimental configuration, it is typically observed that 3 to 4 radial cracks propagate radially after ignition and that such cracks may subsequently bifurcate. Other configurations of the MCCO experiment produce results that are a bit different from

those discussed here. For the purpose of validating the numerical models, this particular configuration is the only one that has been numerically modeled to date.

## Numerical Model

The time scale of the experiment is on the order of $10^{2}$ seconds for the heat-up phase and on the order of $10^{-6}$ seconds for the chemically reactive phase. This variation in time scales makes necessary a numerical technique that can undertake large time steps for part of the time and small time steps thereafter. In addition, the complex nature of the experiment requires a non-linear model. With these requirements in mind, the implicit finite element method was chosen as the framework for the current work. The upper and lower constraints on the HE and confinement ring do not allow significant straining in the axial direction, therefore, a two-dimensional plane strain model is sufficient.

Within the two-dimensional non-linear implicit finite element framework, many phenomena must be incorporated to accurately model the MCCO. As the sample assembly is heated, the free thermal expansion of the HE would be greater than that of the metal. In the constrained state, this expansion mismatch causes a stress state in the metal that exceeds the material's yield strength. During the heat-up phase, the HE produces decomposition gases. For the wire-ignited (as opposed to auto-ignited) specimens, a pressure due to the ignition of these gases is generated in the HE cavity. This large pressure causes tensile hoop strain in portions of the HE, which, in turn, causes discrete cracks to form that propagate radially outward. As these discrete cracks open up and propagate, the gas pressure also acts on the crack faces and applies an additional

crack opening load. The entire process is extremely dependent on the mechanical and thermal nature of the PBX 9501, which is a history and rate-dependent nonlinear material that has complex constitutive behavior. To summarize, the features that must be included in the numerical model are:

1. thermal expansion,
2. metal plasticity,
3. mechanical loading,
4. discrete cracking, and,
5. constitutive behavior model for PBX 9501.

It is hypothesized at this juncture that the features listed above are the most significant ones in the experiment and an accurate numerical model including these features will generally characterize the results of MCCO experiments. However, there are other features of the MCCO that are thought to be important, but are not included in the current numerical model. Liu [9] proposed a concept called stress-bridging to describe an observed microscopic behavior of PBX 9501 which is characterized by the formation of a "damage zone" ahead of a macroscopic crack before and during crack propagation. At present, Fourier heat conduction is left out of the FE model because it is the opinion of the authors that it has little effect. Models for gas production and the associated combustion and pressure do exist [10, 11], but such models are not included at this time. Also, mechanical loading of sub-continuum features may be important, but models for such phenomena are not included.

While these features have not been included in the numerical model presented, the results presented later in this paper indicate that they may not be major factors in the

overall behavior of the experiment. However, some, or perhaps all, of these features may need to be included in future numerical models to more accurately predict the behavior of the MCCO experiment. Also, it is not at all certain that all of the important factors have yet been identified.

Thermal expansion, metal plasticity and mechanical loading are incorporated into this finite element model with relative ease therefore their implementation is not discussed here. Discrete cracking and the material model of PBX 9501 are relatively new models so discussion of some of the details of these two models is included in the following.

## Discrete Cracking

A brief description of the model for discrete cracking developed by Gerken [8], with some modification to allow for material non-linearity, is presented here. The model allows for discrete crack propagation along any pre-existing finite element edges, thereby allowing discrete crack propagation along arbitrary paths without the need for *a priori* assessment of the crack paths. The model has been incorporated as a User Element into the implicit finite element code ABAQUS/Standard.

### Conceptual Development

Shown in Fig. 3a is a representation of a simple mesh of the type used in this analysis. Every element is defined by unique nodes. Figure 3b shows the four unique nodes that occur at an interior point at which 4 elements have a common nodal location.

These coincident nodes are condensed in an ABAQUS user Multi-Point Constraint subroutine to maintain displacement continuity across each interface. As a discrete crack propagates along element interfaces, the elements can separate and still maintain their original nodal connectivity.

Figure 3c shows the conceptual representation of a single element with cracks at 4 interfaces. The two-dimensional finite element equations are developed via the Hu-Washizu Energy Principle [12]. To apply the Hu-Washizu Energy Principle in this case it is necessary to derive the stiffness matrix and load vector for the FE and cracks combined. In order to do this, the problem is treated as a single FE with a single crack. Then, additional cracks are superimposed as indicated in Fig. 3c for the case of 4 interface cracks. The dashed representation of 3 of the elements in 3c indicates that the stiffness of the element is incorporated only once. Figure 4 shows the basic fracture mechanics problem that is analyzed to provide the information needed to conduct the superposition shown in Fig. 3c.

Finite Element Development

The Hu-Washizu Energy Principle has the form

$$\Pi_{HW}(\mathbf{u},\boldsymbol{\sigma},\boldsymbol{\varepsilon}) = \int_{\Omega}\left[\frac{1}{2}\boldsymbol{\varepsilon}^{\mathrm{T}}\mathbf{D}\boldsymbol{\varepsilon} - \boldsymbol{\varepsilon}^{\mathrm{T}}\mathbf{D}\boldsymbol{\varepsilon}_0 + \boldsymbol{\varepsilon}^{\mathrm{T}}\boldsymbol{\sigma}_0 + \boldsymbol{\sigma}^{\mathrm{T}}(\mathbf{L}\mathbf{u} - \boldsymbol{\varepsilon})\right]\mathrm{d}\Omega - \Pi_{EXT} \qquad (1)$$

where the independent variables **u**, $\boldsymbol{\sigma}$, and $\boldsymbol{\varepsilon}$ are displacement, stress and strain respectively, $\Omega$ is the element volume (or area for a two-dimensional element), **D** is the elastic moduli coefficients matrix, $\boldsymbol{\varepsilon}_0$ and $\boldsymbol{\sigma}_0$ are the initial strain and stress tensors respectively, $\Pi_{EXT}$ is the external work, and **L** is the strain displacement operator. To

incorporate the effects of the edge cracks into the formulation, the external work term, $\Pi_{EXT}$, is assumed to include an external strain field applied to the element. This external strain field is the strain field in the element due to a small crack on its surface. Shown in Fig. 4, this strain field is determined by analyzing a small crack in an infinite linear elastic plate subject to the far-field stresses shown. The strain field in the element due to the crack can be obtained analytically and included in the external work term, $\Pi_{EXT}$.

It can then be shown by taking the first variation of $\Pi_{HW}$ and making appropriate approximations for **u**, $\boldsymbol{\sigma}$, and $\boldsymbol{\varepsilon}$, that the following matrix equation results

$$\mathbf{Kd} = \mathbf{f} + \mathbf{F}_0 + \sum_{i=1}^{n} \mathbf{Q}_i \ , \tag{2}$$

where **K** is the stiffness matrix, **d** is the vector of nodal displacements, **f** and $\mathbf{F}_0$ are the body force and initial condition load vectors and $\mathbf{Q}_i$ is the additional load vector due to a single small crack on the element edge, with *n* being the number of edge cracks. If there are no interface cracks, $\mathbf{Q}_i \equiv \mathbf{[0]}$ and Eqn. 2 simplifies to the standard two-dimensional finite element equations derived from the Hu-Washizu Energy Principle.

It should be noted that in Gerken's work [8], the initial stress and strain are assumed to be zero. While this may be true if the elastic moduli coefficients matrix, **D**, is taken to be the equivalent secant moduli matrix, it is not true for an incrementally linear solution to a non-linear problem, the solution method in ABAQUS/Standard. In this case **D** is the equivalent tangent moduli matrix. Hence, for use in the numerical model presented here, the initial condition load vector, $\mathbf{F}_0$, has been taken into account, where $\boldsymbol{\varepsilon}_0$ and $\boldsymbol{\sigma}_0$ are relative to the current solution increment, not the initial conditions at the start of the solution.

Fracture and Separation

By defining each element with unique node numbers, the elements can separate from adjacent elements and still maintain their original nodal connectivity. This separation simulates the geometrical aspects of discrete crack growth. To accurately model the fracture process, appropriate failure criteria for interface failure must be defined so that the interface separation reproduces the correct physics of the solution. Because it is difficult to evaluate global fracture criteria without prior knowledge of the solution, a local failure model has been developed based on information available in the simulation at the interface level (i.e. solution variables from the two adjacent elements).

The definition of two adjacent elements with a small crack located at their interface allows for the application of classical elastic/plastic fracture mechanics on a local scale. The small crack at the interface can be approximated to behave like a small crack in an infinite elastic plate. The far field stresses acting on the infinite plate are assumed to be the average stresses from the edges of the two adjacent elements so that the local strain energy release rate can be determined from the following equations:

$$K_I = \bar{\sigma}_I \sqrt{\pi \cdot a}\,,$$

$$K_{II} = \bar{\tau}_{II} \sqrt{\pi \cdot a}\,,$$

$$G = \frac{K_I^2 + K_{II}^2}{E}, \qquad \text{(3 a, b, c)}$$

where the overbar denotes averaged quantities, $\sigma_I$ and $\tau_{II}$ are tensile and shear stresses, and $a$ is the interface crack half-length, and $E$ is the elastic modulus of the material. The

growth of the small crack is assumed to be governed by an R-Curve based on G. The strain energy release rate is assumed to be in the form

$$G = \beta(\Delta a)^{\gamma} + \lambda, \tag{4}$$

where $G$ is the strain energy release rate, $a$ is the crack half width, and $\beta$, $\gamma$, and $\lambda$ are curve fitting parameters. Equation 4 can then be rearranged to give the change in crack length given the strain energy release rate and the other parameters in the form

$$\Delta a = \left( \frac{G - \lambda}{\beta} \right)^{\frac{1}{\gamma}}. \tag{5}$$

Hence, given the stresses from the two adjacent elements, the local strain energy release rate is determined. Then, at the end of a time step in the finite element simulation, the change in crack length of the interface crack is determined. If the interface crack grows to be wider than the length of the element edge, the interface fails and is allowed to separate by not enforcing the multi-point constraint on the adjacent interface nodes. As the simulation progresses, the failed interfaces coalesce into macroscopic cracks.

This model applies standard fracture mechanics ideas to cracks at the size scale of the interfaces. While such an approach may not be fully applicable, the simulations presented in this paper will show that the qualitative aspects of the experiment are reproduced. It should be noted that while element separation to model fracture has been done previously [13 - 15] this formulation provides an alternate approach that uses fracture mechanics concepts on a local scale to simulate growth of interface cracks that coalesce into macroscopic cracks.

ViscoSCRAM

Another significant part of the numerical model of the MCCO experiment is the constitutive behavior of PBX 9501. The ViscoSCRAM material model has been developed to model the following observed characteristics of PBX 9501; 1) irreversible material damage, 2) visco elastic material response, 3) adiabatic mechanical heating, 4) chemical heating, 5) non-shock ignition. While there probably are other processes that occur in PBX 9501, the incorporation of the mechanical and thermal responses listed above into ViscoSCRAM captures the gross behavior over a wide range of scenarios. This material model is a relatively new constitutive model of PBX 9501. It has been developed by Bennett et al. [16] for explicit finite element applications and by Hackett and Bennett [7] for implicit finite element implementations. The underlying principles of both methods are identical. However, the implicit model is of interest here, therefore, a brief description of the model developed by Hackett and Bennett is presented.

The mechanical response portion of ViscoSCRAM is accomplished by coupling an isotropic material damage model with an isotropic, generalized Maxwell visco elastic model. Shown in Fig. 5 is a one-dimensional conceptualization in which the visco elastic model is a spring connected in parallel with several spring / dashpot elements, this is then connected in series with the damage model. In the figure, **S** refers to stress, **G** refers to stiffnesses, and $\boldsymbol{\eta}$ refers to viscous response parameters. The total deviatoric strain rate is then the sum of the visco elastic deviatoric strain rate, $\dot{\boldsymbol{e}}^{v}$, plus the deviatoric damage strain rate, $\dot{\boldsymbol{e}}^{cr}$. This generalization is assumed to apply in three dimensions. The theoretical development is somewhat involved so the reader is referred to further

explanation that is provided in references [7, 16]. It is important to note that ViscoSCRAM has been carefully validated for PBX 9501 using results from several experiments.

The effects of internal thermal generation are also included in ViscoSCRAM. In the model, internal generation is caused by mechanical work and by chemical decomposition due to both temperature and loading effects. To simulate these thermal effects, an energy balance is formulated that includes the effects of adiabatic compression heating, inelastic work, microscopic damage, and bulk chemical heating. Again, the reader is referred to references [7, 16] for details.

MCCO Model

Shown in Fig. 6 is a plane strain model of the copper confinement ring and the HE that was developed for this analysis in ABAQUS/Standard (ABAQUS). The HE has an inner diameter of 3.175 mm and an outer diameter of 25.4 mm. The inner diameter of the copper ring matches the outer dimension of the HE with the thickness being 3.175 mm giving an outer diameter of the confinement ring of 31.75 mm. The HE consists of 1200 discrete fracture elements. The radial dimension of the HE elements varies from 0.24 mm at the inner row of elements to 0.87 mm for the outer row of elements. The tangential dimension of the HE elements varies from 0.17 mm for the inner row to 1.33 mm for the outer row. Because it has not been observed in the experiments, it is assumed that the copper confinement ring will not crack, therefore, standard plane strain elements are used to model the confinement ring. The confinement ring consists of 180 ABAQUS

plane strain elements. The interface between the copper and the HE is a continuous mesh to model an infinite strength bond. The interface is allowed to deform, but no relative motion between the HE and the copper is allowed. This approximation to the interface behavior is deemed appropriate because relative motion between the copper sleeve and HE was not observed in the experiment.

The copper used in the experiment is oxygen free copper. An isotropic elastic plastic material model was used to model the response of the copper. This material typically has an elastic modulus of 117 GPa and a Poisson's ratio of 0.33. The constitutive behavior was modeled using a power law with a yield stress of 65 MPa, a strain hardening exponent of 0.2 and a yield stress coefficient of 292 MPa. The coefficient of thermal expansion of copper is a constant $16.56 \times 10^{-6}$ /°C and the density is $8.9 \times 10^{3}$ kg/m$^3$.

The ViscoSCRAM constitutive model was used to represent the behavior of the PBX 9501. The constant coefficient of thermal expansion for PBX 9501 is $55 \times 10^{-6}$ /°C and the density is $1.849 \times 10^{3}$ kg/m$^3$. For the conditions of the experiment, it is likely that the material properties are not constant. However, for this work, they are taken to be constant throughout the entire temperature range.

For the discrete fracture model, each element interface in the HE has been seeded with a small crack to simulate the presence of many crack initiation sites in HE. Lacking hard information concerning the sizes of defects in HE, it was necessary to estimate these sizes. It was assumed that these sizes are randomly distributed according to an approximately flat distribution such that the mean crack size is about half the width of the smallest element. Initial crack sizes range from approximately 90 % of the smallest

element width to approximately 10 % of the smallest element width. This size range corresponds roughly with the 10 and 100 micron bimodal distribution of particle size in PBX 9501. This variation in crack sizes also allows for the failure conditions for fracture to be different for each interface. In other words, the interfaces with large cracks will fail "easily", but the interfaces with small cracks require higher levels of stress to fail. Also, by choosing several different sets of samples to represent the same flat distribution and mean crack size, the relationship between the general features of the results and any particular set of interface cracks can be ascertained. It should also be noted that no attempt was made to maintain a constant density of cracks throughout the mesh so that the density of cracks in the finer mesh regions is greater than that in the coarse mesh regions.

The fracture properties of PBX 9501 have been estimated based on the limited information that is available. As a starting point, the fracture data were estimated based on Brazilian disk type fracture experiments performed on "mock" HE [17]. This information was then used to model a three-point bend fracture experiment on PBX 9501. Then, to match the force – displacement results of the three-point bend experiment, the data obtained for the "mock" HE was modified to obtain the fracture properties of PBX 9501. These modified fracture properties were used in the present simulation to model the fracture behavior of the HE. By this process, the fracture parameters in Eqn. (4) were determined to be $\beta = 2.0$, $\gamma = 0.1$, and $\lambda = 0.0$.

The interface failure criteria of Eqns. (3a, b, c) have been modified for this simulation to exclude shear contributions. This is partially due to the difficulties in modeling shear deformation with bilinear finite elements. Bilinear elements can

incorrectly interpret deformation that causes a change of the angle between adjacent sides of an element as shear. This error, coupled with the extremely low fracture toughness of PBX 9501, tends to cause prediction of disperse shear cracking that is inconsistent with experimental results. Because the deformation in the experiment is dominated by primarily mode I type loading, it is not felt that the exclusion of shear stress from the discrete fracture criteria will cause significant error in modeling. It is assuredly the case that the crack propagation response of the PBX 9501 is still not well understood and that the model used in this simulation is the best fracture model that is available.

To reproduce the conditions of the experiment, the analysis simulated heating from room temperature at a rate of 0.6 °C/sec for 200 seconds. During this heat-up phase, only the mechanical response of the HE is enabled. The large time scale of this phase would allow ample time for the entire apparatus to come to thermal equilibrium so the chemical and mechanical heating modeled in ViscoSCRAM was neglected. During this heat-up phase, HE decomposition gases are generated and are then ignited by the NiCr wire. No attempt was made to model this gas generation and ignition process and the resulting pressure pulse, therefore, it was necessary to estimate this pressure pulse based on strain gage data from the MCCO tests [6]. The estimated pressure pulse was taken to be a linear increase at the rate 5 MPa/$\mu$sec which was applied to the inner circumference of the HE throughout the simulation following the heat-up phase. This internal pressure causes a tangential tensile stress to develop in the HE and, as a result, cracks begin to open. As these cracks open, the model instantly applies this pressure to the crack faces.

To take advantage of the implicit finite element formulation during the heat-up phase, the initial time step was set as high as 10 seconds. This time step is then reduced to 0.1 seconds as the end of the heat up is approached. At the beginning of the pressurization, the time step is further reduced to $5 \times 10^{-7}$ seconds. Then, before the fracture criteria for discrete fracture are met, the time step is reduced to $1 \times 10^{-7}$ seconds. As the simulation progresses, this time step can be further reduced by the ABAQUS code if convergence criteria are not met.

## Results

The numerical results of the simulations provide validation of the numerical models. In addition, several processes are thought to occur in the MCCO experiment that were not specifically measured. These simulations provide insight to these processes. The numerical model consists of two different phases; the heat-up phase and the reactive phase. The heat-up phase is a relatively long-time event that is characterized by slow material straining with the build up of stresses. The reactive phase, initiated after the heat-up phase, consists of very short-time events including discrete fracture, mechanical and thermal heating, and high-rate deformation.

During the heat-up phase of the experiment, both the confinement ring and the HE thermally expand. Because the coefficient of thermal expansion of HE is greater than that of copper, the copper ring serves as a restraint to the expansion of the HE. Shown in Fig. 7 are the effective stress contours in the model after a heat up of 120 K. The high effective stresses on the inner surface in Fig. 7a are due primarily to high compressive tangential stresses. While none of the elements has sustained enough damage to start to

soften at the end of the heat-up phase, the inner row of elements has sustained enough damage so that it no longer supports as much stress as the next row of elements. The high stresses in Fig. 7b are due primarily to high tensile tangential stress. These stresses are high enough that the entire ring has exceeded the elastic limit before the end of the heat-up phase. At this stage in the experiment, the model is approximately axi-symmetric, with no tangential variation in material state. Although there are small variations in element behavior due to interface cracks, the variations are not of great enough magnitude to be distinguishable.

After the heat-up, the pressure pulse (5MPa/$\mu$sec) is applied to the inside of the HE. As this pressure is applied, the inner material starts to move radially outward. The acceleration of this outward movement tends to cause additional tangential compressive stress to build up in the inner row of elements. There is a tendency for the compressive stresses in this inner row of elements to not be overcome. In such cases, these elements do not satisfy the discrete fracture criteria and do not separate. However, the compressive stresses due to heat up are overcome in other rows of elements. As the pressure is increased, the stresses in the second (from the inner surface) row of elements transitions to tension. This tension creates strain energy that causes the interface cracks to eventually fail, starting with the largest interface crack. As cracks fail and open up, tensile stresses in the vicinity of the crack are relieved, thereby reducing the strain energy in nearby elements. In addition to relieving nearby tensile stresses, these discrete cracks also create large stress concentrations in front of the crack, encouraging further growth in the radial direction. Crack growth is further encouraged by the application of the internal pressure to the crack faces, which increases the tensile stress acting on the crack. Shown

in Fig. 8 is a graphic of a typical simulation in which many small discrete fractures appear early in the simulation after the pressure is applied. Also note that none of the inner row of elements has fractured. While the random nature of the interface starter crack sizes produces some variability in the results, a different set of samples with the same distribution and mean crack size produces generally the same results.

As simulated time progresses, some of these small cracks will continue to propagate radially outward and some will arrest. The cracks that propagate to become large cracks are thought to be the cracks that would be visible in the experimental photographs. In all of the simulations run to date, 3 – 5 large cracks appear and propagate from near the inner surface to near the copper confinement ring with several smaller arrested cracks. As a crack tip gets close to the confinement ring, the simulated bond between the copper and the HE is probably not an accurate representation of the experimental conditions, therefore, as the discrete cracks near the confinement ring, the solution may not be accurate. Shown in Fig. 9 is a plot of the final deformed shape (with no displacement magnification) of a typical simulation in which 3 large cracks appear. The time in the simulation is 28.8 $\mu$sec after the heat-up, corresponding to an internal pressure of 144 MPa. This time corresponds roughly to the "observation time" reported for the MCCO in which luminescence typically reaches the confinement ring at about 10 to 20 $\mu$sec after the start of observation.

It is important to note in Fig. 9 that some of the elements along the inner row appear to be overlapping. This raises the concern that they may have inverted. However, the material in this region is in a state of advanced damage and would have very little

stiffness, thus even total removal of these elements would have little impact on the features shown in Fig. 9. This point will be addressed again later.

The simulation also provides some insight into processes that are not directly observed by the techniques used in the experiment. It is known that PBX 9501 undergoes decomposition and a temperature rise due to sudden pressure application such as in the MCCO experiment [18]. This can be seen in the numerical model as a significant temperature increase in the HE near the inner surface accompanied by a small increase in temperature relative to the surrounding material near the discrete crack faces. Shown in Fig. 10a is a contour plot of the temperature in the HE at the end of a simulation. It shows an increase in temperature from 413 K at the end of heat up to 450 K at locations on the inner surface. It can also be seen that the HE in the region of the large discrete cracks has increased in temperature relative to the surrounding HE. This heating is due to both mechanical work and chemical decomposition.

Shown in Fig. 10b, the simulation predicts an even more pronounced increase in the damage variable in these areas. The damage variable is a measure of the residual strength of the HE. The damage variable has an initial value of $3 \times 10^{-5}$, corresponding to full strength and an increase in the damage variable corresponds to a decrease in residual strength. It increases to a value of $3 \times 10^{-3}$ at both the interior surface and the area of the discrete cracks indicating a large decrease in residual strength in these locations.

While no attempt has been made to compare the simulation results with either strain gage or interferometry data recorded during the experiments [6], the simulations show that there is significant tangential variation in the strain in the copper confinement ring. Shown in Fig. 11, the plastic strain in the copper is much lower in the regions in

which a large discrete crack has propagated out near the confinement ring. The tangential variation in plastic strain is more pronounced on the inner surface of the ring, but the variation on the outer surface of the ring would be enough to produce significant differences in the strain measurement, depending on the strain gage's proximity to the large cracks.

Numerous simulations have been conducted and they are found to be quite reproducible in terms of the general behavior. Shown in Fig. 12 are four different simulations. Each model is the same except that different sets of random crack sizes, with the same distribution and mean size, have been used to seed the element interfaces. The models show that 3 to 5 large cracks appear and propagate out toward the copper ring. In addition, the total simulation time is similar in all cases with the times relative to the end of the heat-up phase being: a) 27.4 $\mu$sec, b) 26.9 $\mu$sec, c) 29.0 $\mu$sec, and d) 28.8 $\mu$sec. Also, each of the simulations show that both the general distribution and magnitude of the temperature and damage are similar to that reported above (i.e. both temperature and damage are high on the pressurized exposed HE surfaces).

It is noted that Fig. 12d is the same as Fig. 9 in which it was pointed out that some of the elements may have inverted. Similar behavior is observed in the other simulations in Fig. 12 as well. In order to determine if this phenomenon is caused by a time step that is too large and to confirm that it has little effect on the results, a simulation was conducted with a time step of $1 \times 10^{-8}$ seconds. This is an order of magnitude smaller than the $1 \times 10^{-7}$ seconds used in the first set of simulations. Figure 13 shows the result of this simulation at about 18 $\mu$sec after the end of heat-up. It shows there is no evidence of element inversion and the general crack pattern seen in the first simulations is retained.

Also retained is evidence that some cracks have started in the second row of elements from the inner surface. This indicates that the effect of the element inversion was insignificant in the first simulations and that they are removed by reducing the time step. It is encouraging that adequate results can be obtained using the larger time step, thus incurring less computational expense.

## Summary and Conclusion

A finite element simulation of the Mechanically Coupled Cook Off experiment on PBX 9501 has been conducted to help validate some of the HE modeling techniques. Photographs from the experiment show the formation of 3 to 5 large discrete cracks that propagate from the inner surface radially outward toward the confinement ring. The finite element model includes the behaviors thought to be essential to modeling the MCCO. Two key components of the numerical model are the ViscoSCRAM material model for PBX 9501 which models both the thermal and mechanical response of the HE and a discrete fracture model which models macroscopic fracture based upon fracture criteria. Much is still not known about the behavior of PBX 9501 and many assumptions had to be made and material information had to be estimated from limited data. In spite of these known shortcomings, the incorporation of ViscoSCRAM and discrete fracture with other standard finite element modeling techniques has produced a simulation of the MCCO that reasonably well reproduces the photographic observations of the experiment.

References

1. McGuire, R.R., and Tarver, C.M., (1981) “Chemical Decomposition Models for the Thermal Explosion of Confined HMX, TATB, RDX, and TNT Explosives”, Proceedings, 7th International Symposium on Detonation, Naval Surface Weapons Center, White Oak, Maryland, pp. 56-64.

2. Dienes, J.K., (1984), “A Unified Theory of Flow, Hot-spots, and Fragmentation with an Application to Explosive Sensitivity”, High Pressure Shock Compression of Solids II: Dynamic Fracture and Fragmentation, L. Davison et al, eds., Springer, New York, pp. 366-398.

3. Field, J.E., Bourne, N.K., Palmer, S.J.P., and Walley, S.M., (1992), “Hot-Spot ignition Mechanisms for Explosives and Propellants”, Philosophical Transactions of the Royal Society of London, A, Vol. 339, pp. 269-83.

4. Howe, P.M., Gibbons, G., Jr., and Webber, P.E., (1985), “An Experimental Investigation of the Role of Shear in Initiation of Detonation by Impact”, Proceedings, 8th International Symposium on Detonation, Naval Surface Weapons Center, White Oak, Maryland, pp. 294-306.

5. Gray, G.T., Idar, D.J., Blumenthal, W.R., Cady, C.M., and Peterson, P.D., (1998), “High and Low Strain Rate Compression Properties of Several Energetic Material Composites as a Function of Strain Rate and Temperature”, To appear: Proceedings, 11th International Symposium on Detonation, Office of Naval Research, Washington, D.C.

6. Dickson, P.M., Asay, B.W., Henson, B.F., and Fugard, C.S., (1998), “Observation of the Behavior of Confined PBX 9501 following a Simulated Cookoff Ignition”, To appear: Proceedings, 11th International Symposium on Detonation, Office of Naval Research, Washington, D.C.

7. Hackett, R.M., and Bennett, J.G. (1999) “An Implicit Finite Element Material Model for Energetic Particulate Composite Materials”, Technical Report, LA-UR-99-3139, Los Alamos National Laboratory, Los Alamos, New Mexico.

8. Gerken, J.M., (1998) “An Implicit Finite Element Method for Discrete Dynamic Fracture”, MS thesis, Colorado State University, Fort Collins, Colorado.

9. Liu, C., Stout, M.G., and Asay, B.W., (1999) “Stress Bridging in a High Explosive Simulant Material”, Technical Report, LA-UR-99-3949, Los Alamos National Laboratory, Los Alamos, New Mexico.

10. Tarver, C.M., McGuire, R.R., Lee, E.L., Wrenn, E.W., and Brien, K.R., (1978), “The Thermal Decomposition of Explosives with Full Containment in One-Dimensional

Geometries", Proceedings, 17th International Symposium on Combustion, Combustion Institute, Pittsburgh, Pennsylvania, pp. 1407-1413.

11. Ward, M.J., Son, S.F., and Brewster, M.Q., (1997), "Steady Deflagration of HMX with Simple Kinetics: A New Modeling Paradigm", Technical Report, AIAA 97-0950, 35th AIAA Aerospace Sciences Meeting & Exhibit.

12. Hu, H.C., (1955), "On Some Variational Principles in the Theory of Elasticity and the Theory of Plasticity", Scientia Sinca, Vol. 4, pp. 33- 54.

13. Xu, X. P., Needleman, A., (1994), "Numerical Simulations of Fast Crack Growth in Brittle Solids," Journal of the Mechanics and Physics of Solids, Vol. 42, pp. 1397-1434.

14. Liaw, B. M., Kobayashi, A. S., Emery, A. F., (1984), "Double Noding Technique for Mixed Mode Crack Propagation Studies," International Journal For Numerical Methods in Engineering, Vol. 20, pp. 967-977.

15. Goodman, R. E., Taylor, R. L., Brekke, T. L., (1968), " A Model for the Mechanics of Jointed Rock," Proceedings of the ASCE: Journal of the Soil Mechanics and Foundations Division, Vol. 98, pp. 637-659.

16. Bennett, J.G., Haberman, K.S., Johnson, J.N., Asay, B.W., and Henson, B.F., (1998) "A Constitutive Model for the Non-Shock Ignition and Mechanical Response of High Explosives", Journal of the Mechanics and Physics of Solids, Vol. 46, pp. 2303-22.

17. Liu, C. Private Communication.

18. Asay, B.W., Funk, D.J., Henson, B.F., and Laabs, G.W., (1997), "Speckle Photography During Dynamic Impact of an Energetic Material Using Laser Induced Fluorescence", Journal of Applied Physics, Vol. 82, pp 1093-99.

# List of Figures

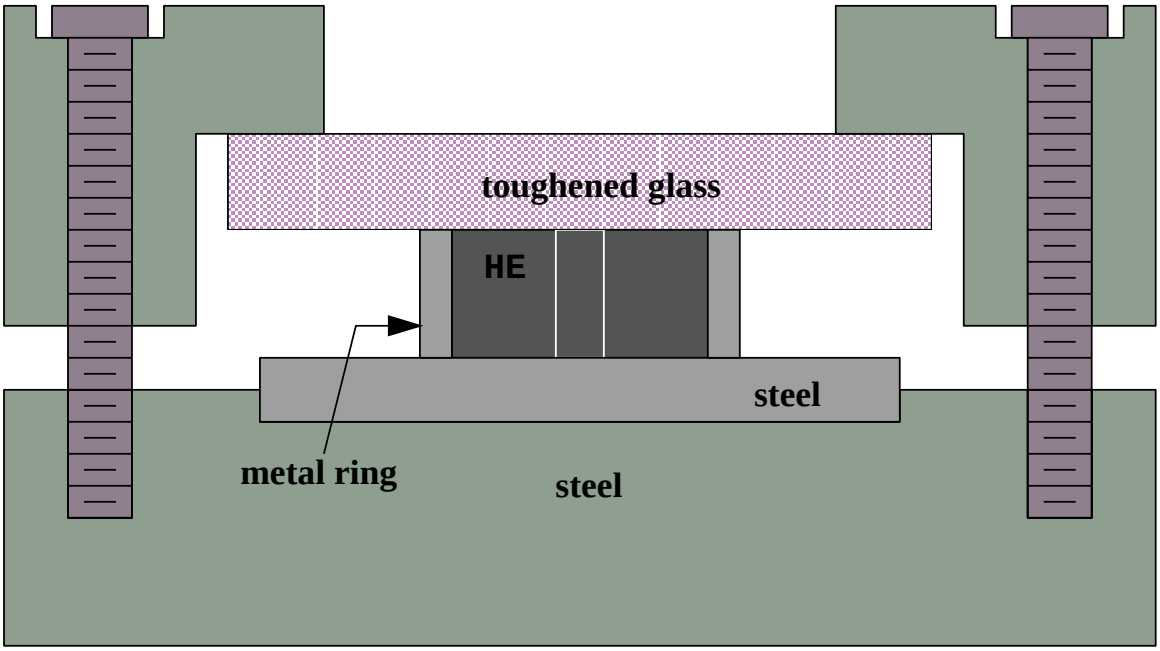


Figure 1. Setup of MCCO experiment.

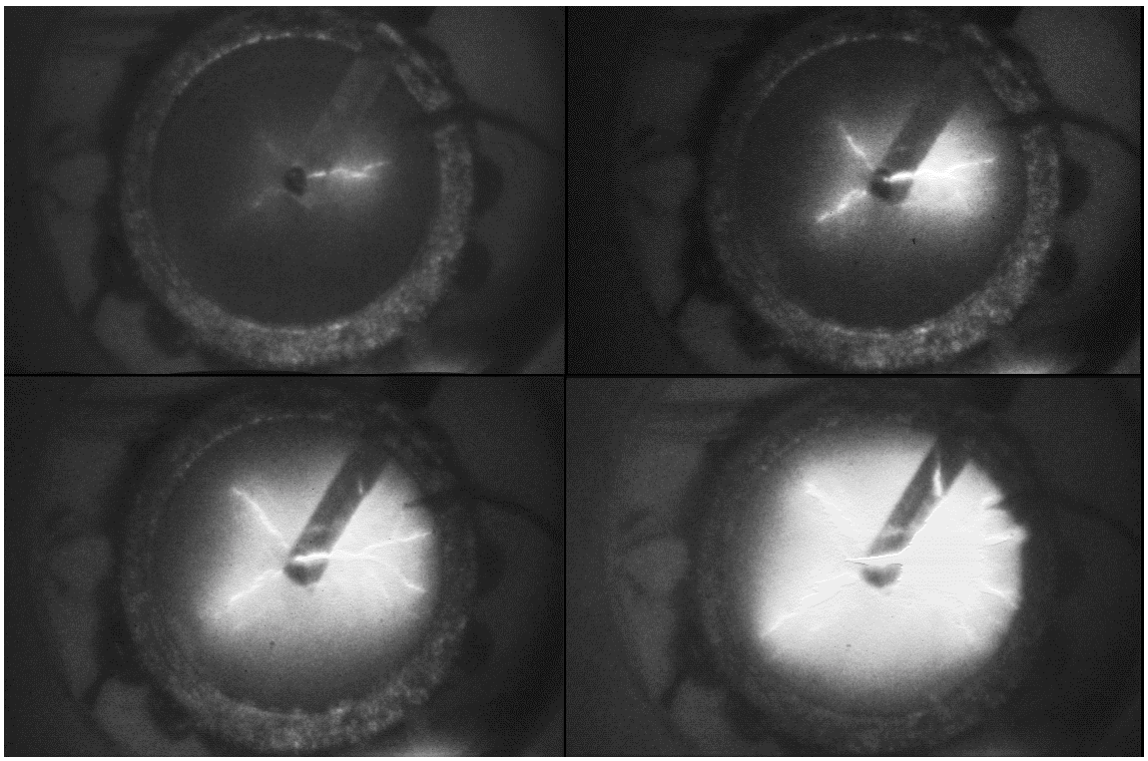

Figure 2. Optical photographs of MCCO experiment. Relative time: upper left: 0 $\mu$sec, upper right: 5$\mu$sec, lower left: 10 $\mu$sec, lower right: 15 $\mu$sec.

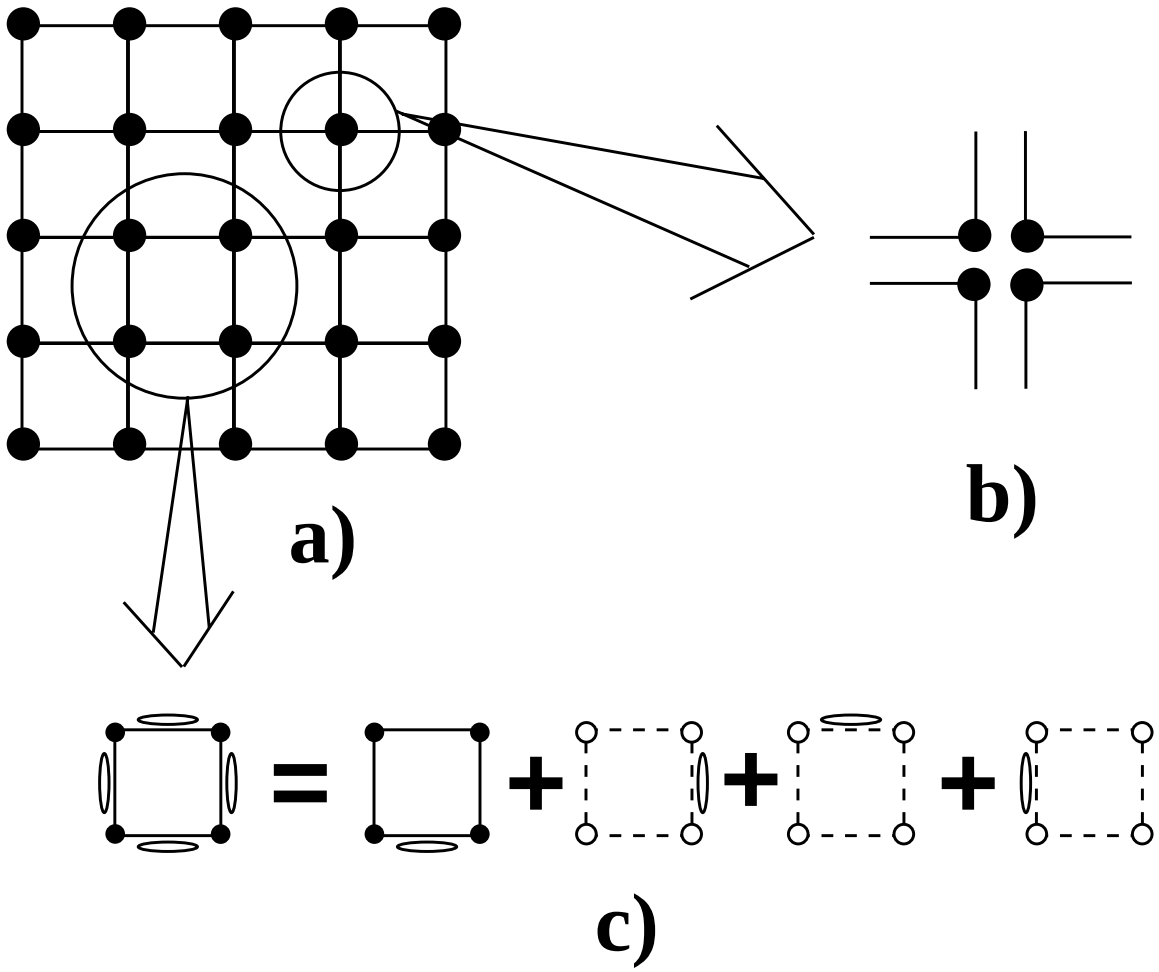


Figure 3. a) Multi-noded FE mesh; b) 4 coincident nodes at an internal nodal location; c) superposition of FEs with interface cracks.

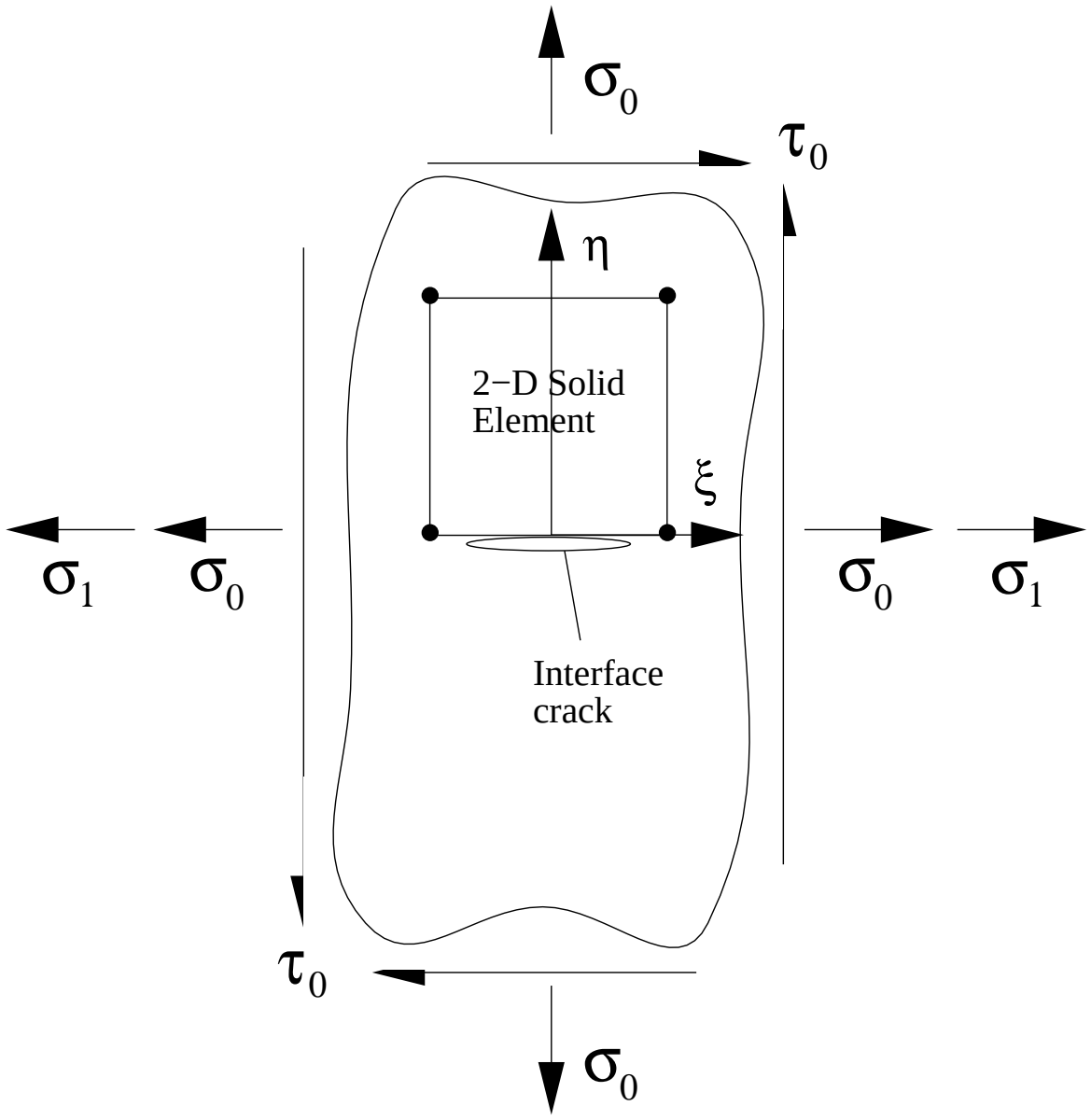


Figure 4. Strain field from a small crack applied to the finite element as external work

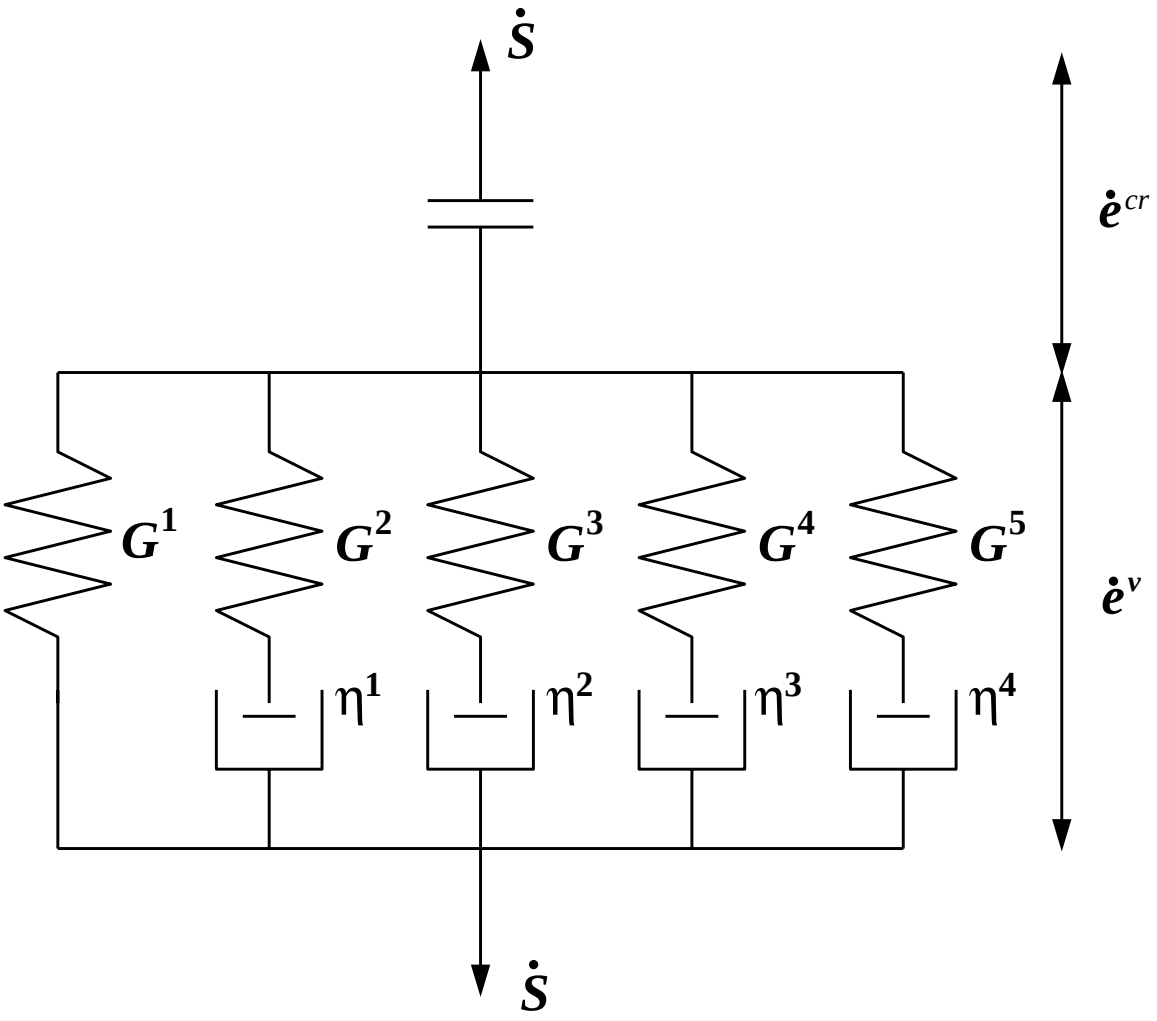


Figure 5. One-dimensional conceptual representation of ViscoSCRAM.

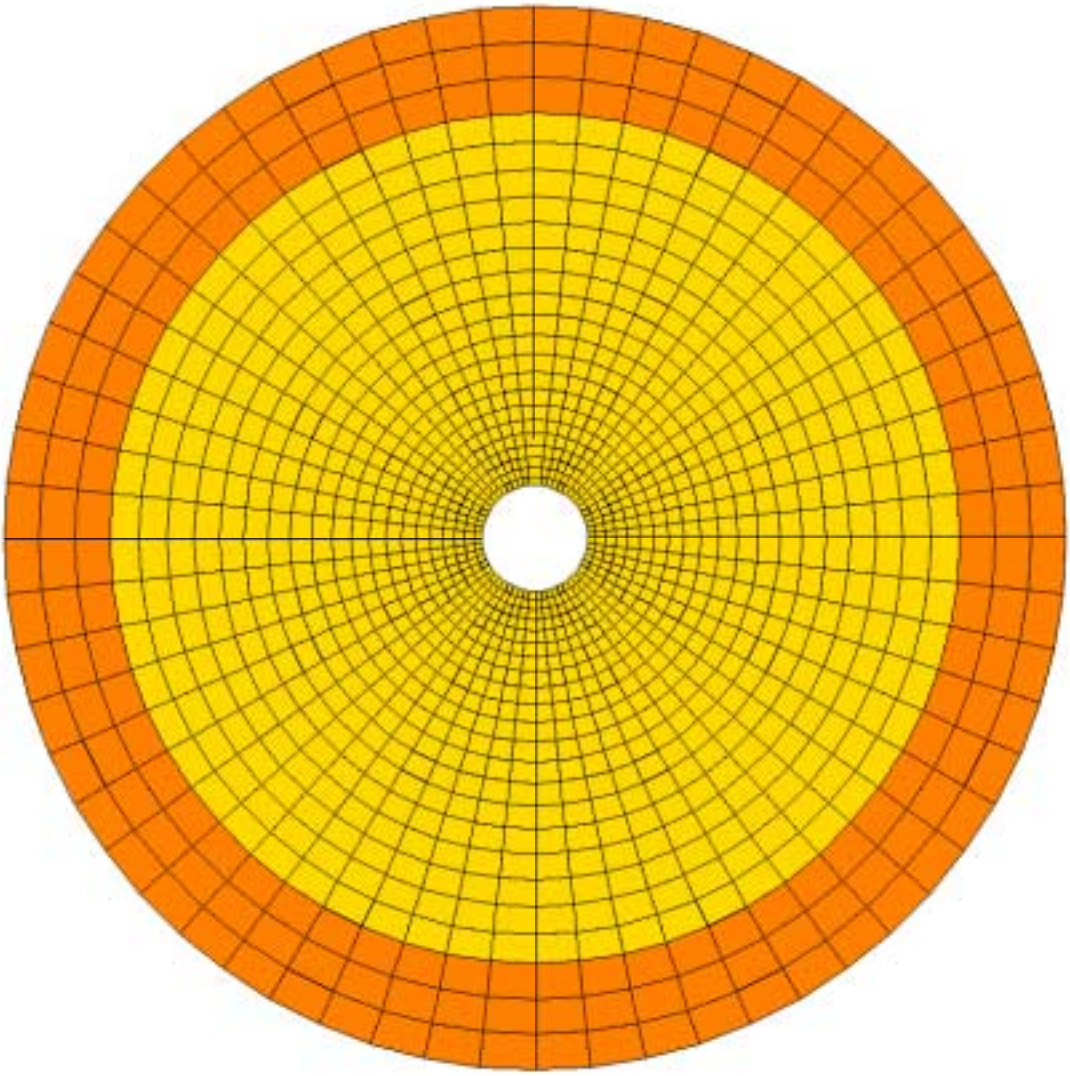

Figure 6. Finite element mesh of the HE and copper ring for the MCCO experiment.

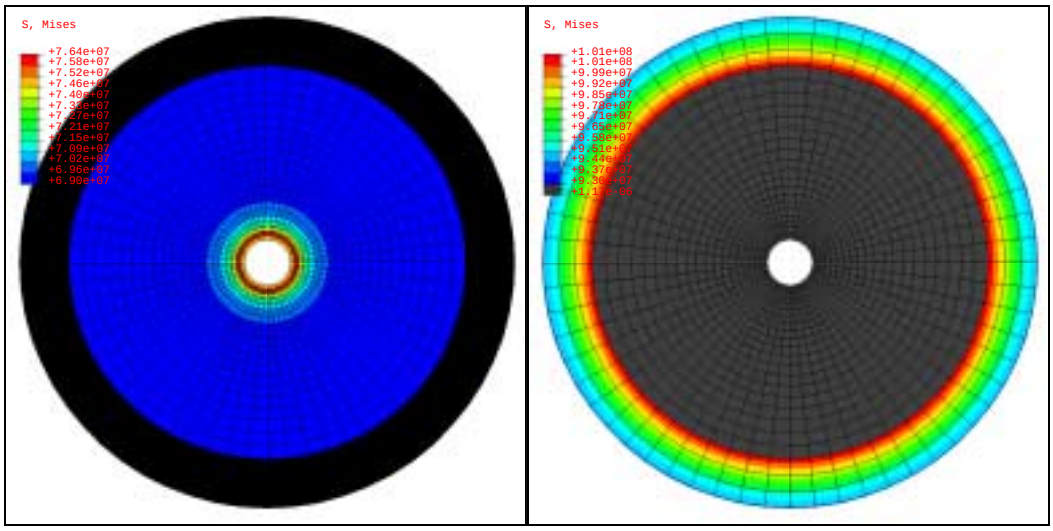


a) PBX 9501 b) Copper Confinement Ring

Figure 7. Effective stress contours for the model after the heat up phase.

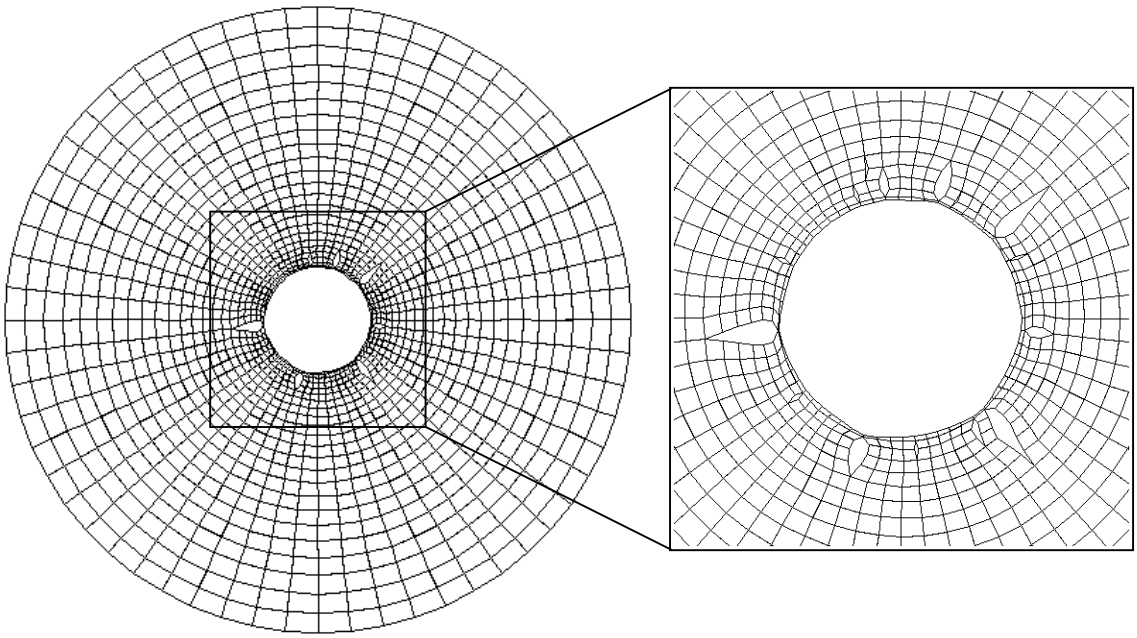

Figure 8. Many small discrete cracks appear near the inner surface of the HE early in the simulation. 10x displacement.

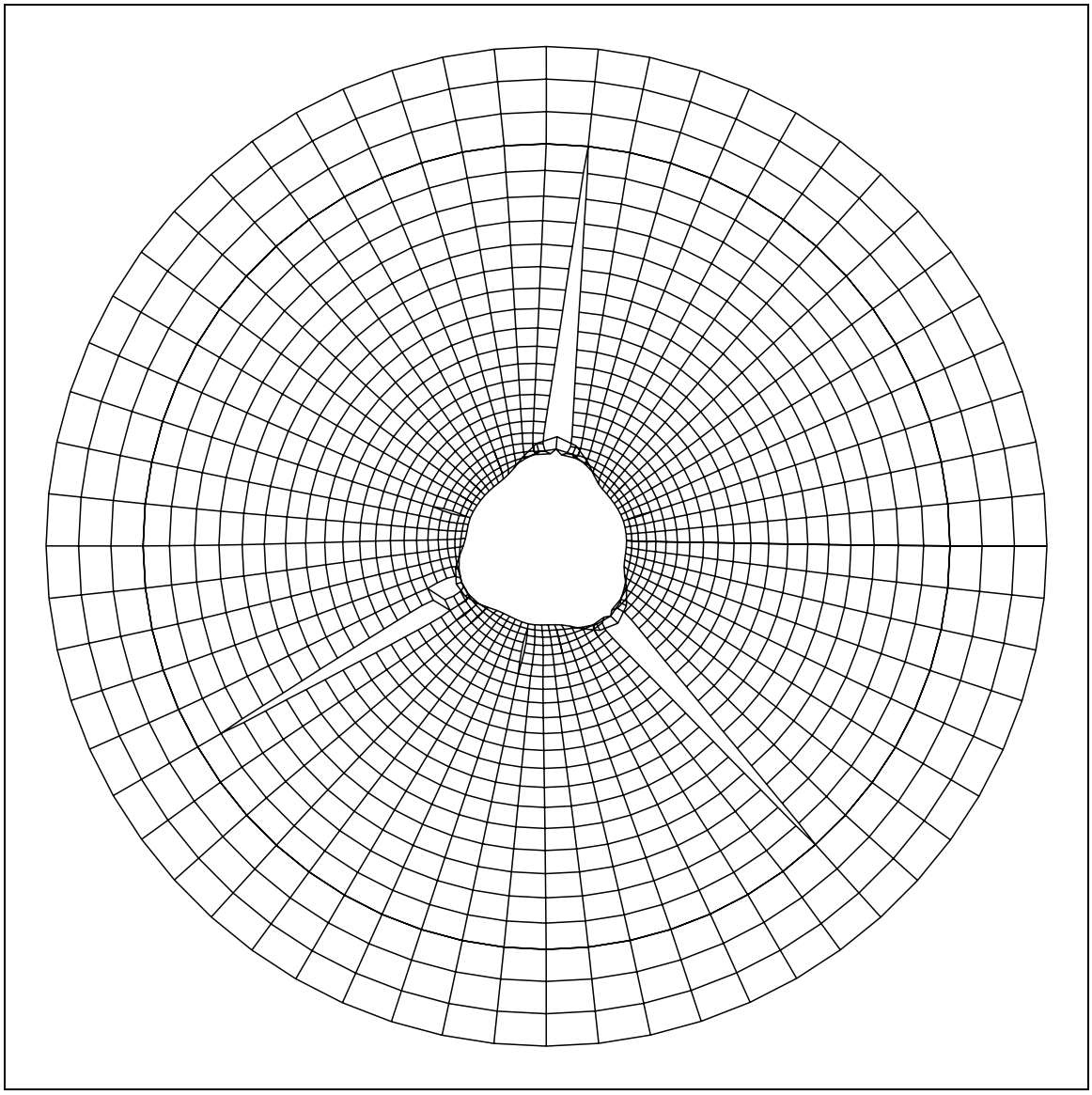

Figure 9. Final deformed shape of an MCCO simulation.

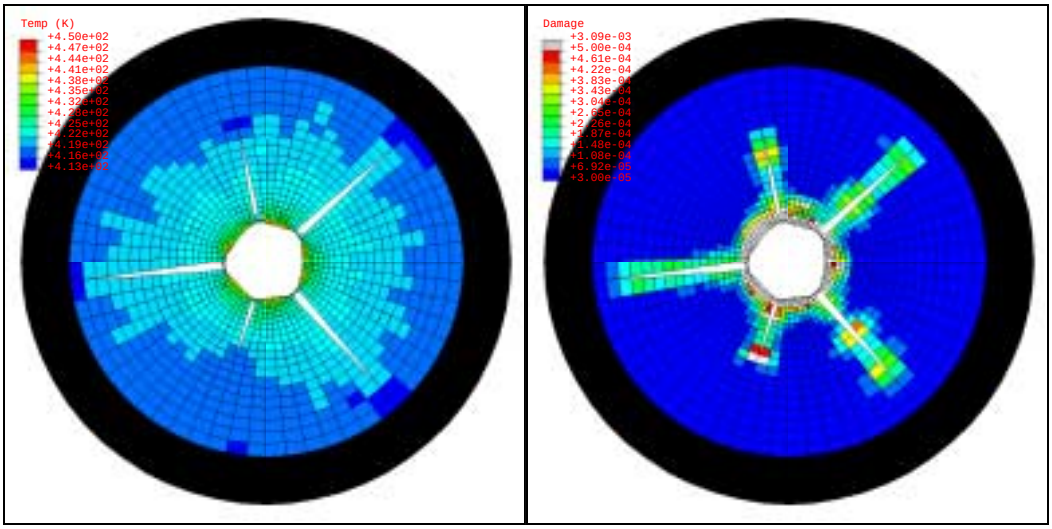


a) Temperature b) Damage

Figure 10. The a) temperature distribution and b) damage in HE at end of simulation shows an increase in both near the inner surface and the large discrete cracks.

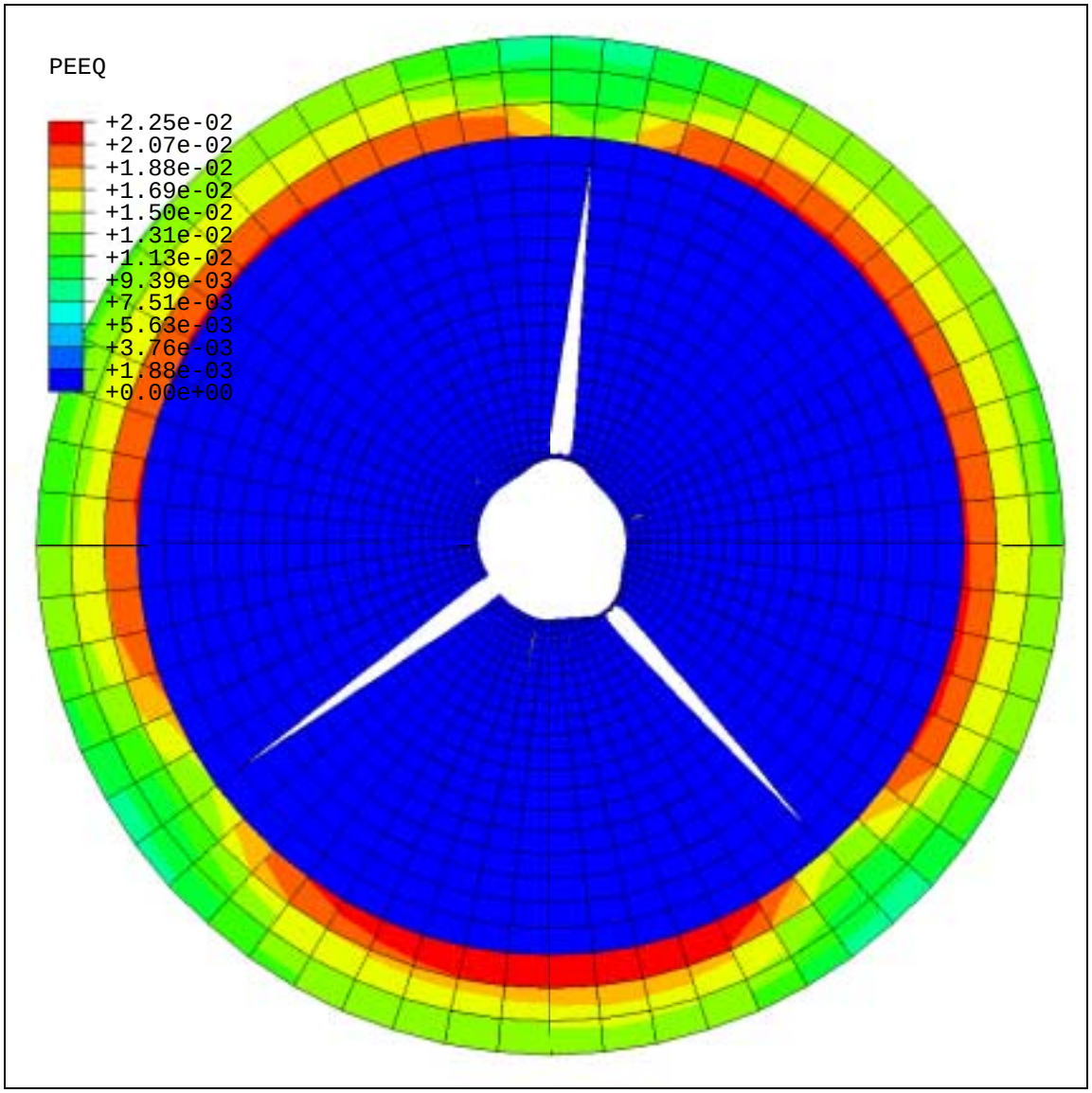


Figure 11. The equivalent plastic strain in the copper confinement ring shows significant tangential variation as a function of the proximity to the large discrete cracks.

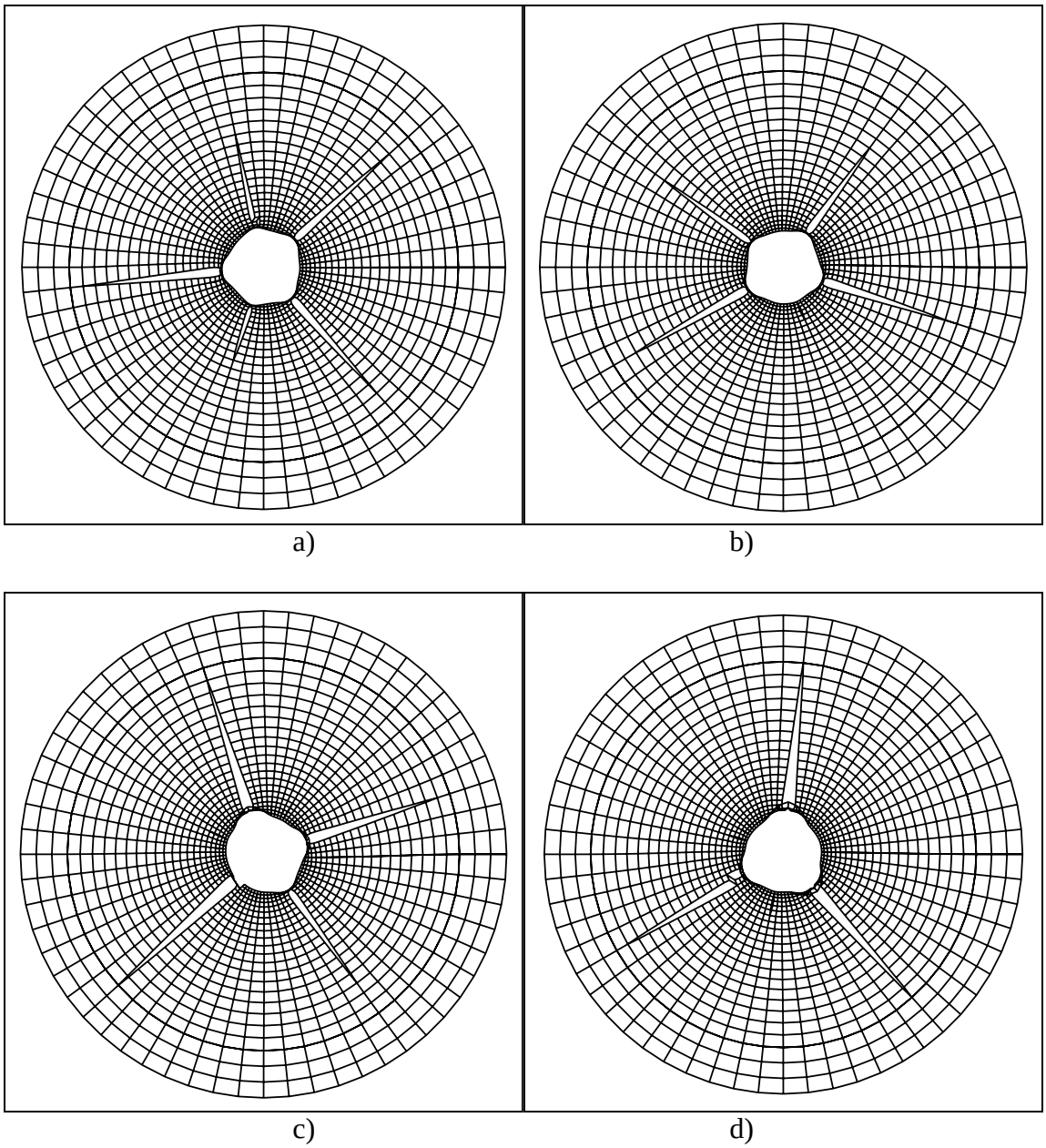


Figure 12. Several simulations show the appearance of 3 –5 large cracks.

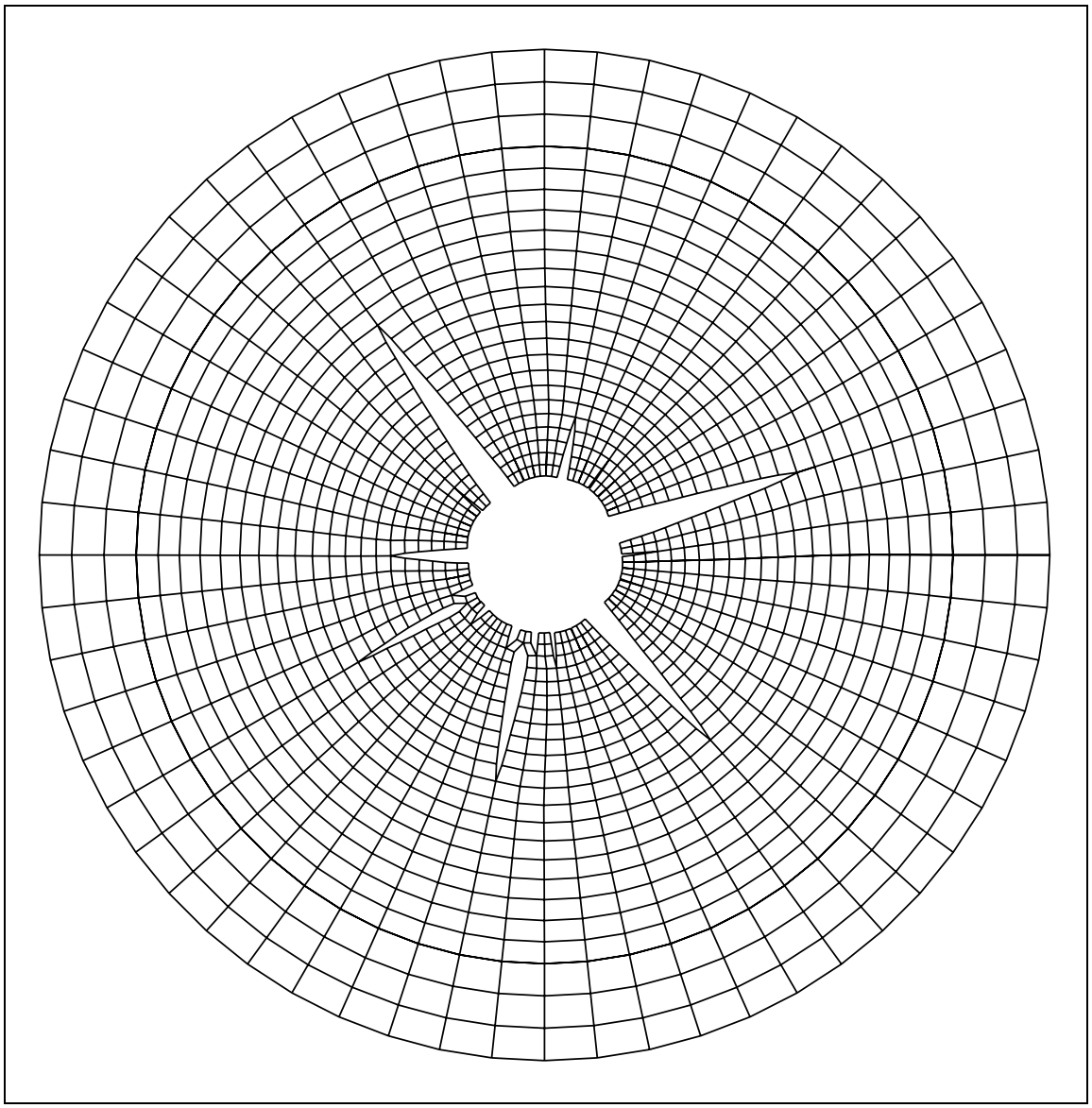

Figure 13. Final deformed shape of an MCCO simulation, short time step. 4x displacement.